Application of LES and binned microphysics for sensitivity study on contrail evolution

W.W. Huebsch*, D.C. Lewellen
West Virginia University, Morgantown, WV, US

Keywords: contrails, LES, binned ice microphysics, sensitivity study

ABSTRACT: A preliminary sensitivity analysis on contrail evolution out to 1000 seconds has been performed using 3-D high-resolution large-eddy simulations to solve the wake and plume development, coupled with a binned ice microphysics model. The aircraft wake dynamics in the first few minutes can have profound effects on the properties of the resulting persistent contrails. This occurs both through its governing of the initial plume dispersion and through the loss of a significant fraction of the ice crystals due to adiabatic heating in the falling wake plume, even at large ambient supersaturation levels. Effects of both atmospheric and aircraft parameters are investigated including relative humidity with respect to ice, ambient stratification, wind shear, and the effective ice crystal emission index. It is shown that the use of binned microphysics can have a significant impact on the prediction for the contrail evolution. The use of the binned microphysics also allowed the simulations to capture a late-time crystal loss due to buoyant oscillations of the plume.

1 INTRODUCTION

Aircraft contrails have gained renewed interest in recent years due to the possible climate impact. It has become increasingly clear that for some conditions aircraft contrails can persist and grow into significant cloud cover that might otherwise be confused with natural cirrus (Minnis, 1998}. It is not uncommon for portions of the upper troposphere to be highly supersaturated with respect to ice and yet be cirrus free until the passage of an aircraft seeds its formation. The projected large increases in air traffic in the coming decades and potential impact of increased cloud cover on global climate change has led to a growing realization of the importance of understanding the formation, properties, and effects of persistent contrails (Penner et al., 1999).

Contrail formation and evolution is not simply a matter of fuel consumption and atmospheric conditions. It is a complex process involving many properties of the ambient atmosphere, the aircraft, and dynamics ranging on length scales from nanometers for the ice microphysics to kilometers for late time atmospheric dispersion. The specific goal of the current research is to investigate the impact of various atmospheric and aircraft parameters on key metrics of contrail evolution from ages of a few seconds out to 1000 s. Large-eddy simulations (LES) with a binned microphysics are employed, extending an earlier LES study with bulk microphysics (Lewellen and Lewellen, 2001).

2 MODEL AND SIMULATION OVERVIEW

Accurately capturing the wake fluid dynamics and its effects on passive species dispersion are important components in correctly modeling contrail evolution. If there were no ice crystal loss, then the local ice crystal number density evolution would be determined (for given distribution at some early time) solely by fluid dynamic advection, until sedimentation became important. For most of this evolution the local ice mass never strays far from equilibrium conditions so it is governed by fluid dynamic mixing as well. Generally there will be some ice crystal loss due to adiabatic heating when parcels descend significantly (Lewellen and Lewellen, 2001; Sussmann and Gierens, 1999) - again a direct consequence of the fluid motions.

* *Corresponding author:* Wade W. Huebsch, MAE Dept., West Virginia University, PO Box 6106, Morgantown, WV, US, 26506-6106. Email: Wade.Huebsch@mail.wvu.edu

To reasonably model the dispersion of the engine exhausts and the basic features of the wake vortex evolution (i.e., how long the vortices persist, how far they drop, and how rapidly the wake volume increases) 3-D high resolution large eddy simulations are used. The model and run procedures are ones employed extensively in previous wake and contrail studies (Lewellen and Lewellen, 2001, 1996). The LES is a finite difference implementation of the incompressible Navier-Stokes equations with the Boussinesq approximation on stretched and staggered grids and second-order accurate in time and space. A piecewise parabolic model (PPM) algorithm is used for the advection of scalars. For the simulations presented in this paper the grids used were on the order of 2.5 million grid points with the finest resolution of 0.4 m and domain sizes up to 1.6 km. Grid independence studies with both finer and coarser resolution showed similar results.

The contrail code has both a bulk and binned option for handling the ice microphysics required for contrail development. The bulk ice microphysics parameterization is a relatively simple model (Lewellen and Lewellen, 2001) and therefore less costly (computationally) than the binned microphysics. In the binned version, the ice microphysics were improved by incorporating components of the NASA Ames Community Aerosol and Radiation Model for Atmospheres, or CARMA (e.g. Jensen et al., 1998). Diffusional growth/sublimation, sedimentation, buoyancy due to latent heat release, and perturbation pressure effects are included in both models.

The contrail simulation is initialized from a 2-D Boeing wake roll-up calculation generated with a Spalart-Allmaras (Spalart and Allmaras, 1992) turbulence model and taken at one second downstream of the B-767 aircraft. The fluid velocities and a passive exhaust tracer are then interpolated onto the contrail grid. The passive tracer is used to distribute the perturbation temperature, as well as the ice crystal and engine water distributions, based on the fuel flow rate, the assumed propulsion efficiency (30%), and appropriate emission indices. Separate LES simulations are used to generate ambient turbulence fields that are added to the contrail field.

Parameter variations are explored starting from the following base case: a wake from a B-767, flying at Mach = 0.8, initialized at one second; assuming fuel flow rate and effective ice crystal number emission index of F = 5.6 kg/km and $EI_i = 10^{15}$ (number/kg of fuel); for ambient conditions at flight altitude of no mean wind shear, stable stratification given by a potential temperature gradient of 2.5 K/km, pressure P = 250 hPa and temperature T = 220 K, and relative humidity with respect to ice RH_i = 110%; simulated with the binned microphysics with a mass ratio between successive ice bins of 3.0, a smallest crystal radius of 50nm, and initial crystal radius of 0.2 μm.

3 RESULTS

In the following we consider in turn how different variables affect contrail metrics such as total ice crystal number and total ice mass per length of flight path. When comparing results from parameter variations, it should be noted that different turbulent realizations produce variations on the order of ~10% (e.g. in ice crystal number density, $N(t)$), which should be used in judging the significance of the differences.

3.1 *Bulk vs. Binned Microphysics and RH_i*

Figure 1 shows the total ice crystal number ($N(t)$ per meter of flight path) at two different ambient supersaturation levels with either the bulk or binned microphysics and illustrates why the added computational cost of the latter is required for many purposes. These results show a dramatic difference in the fraction of crystals lost during the descent of the vortices for the bulk and binned models. Since these crystals are never recovered, this leads to significant differences in contrail properties (e.g., optical depth or mean crystal size) that will persist in time. For the total ice mass and its vertical distribution, the results show only modest differences between the bulk and binned microphysics; these measures are largely governed by the evolution of the plume volume. There is a good physical reason for the greater crystal loss with the (physically more accurate) binned microphysics. As the vortex system falls there is a competition between the temperature rise due to adiabatic compression evaporating the ice crystals, and the mixing with the moist ambient air favoring growth. In the binned microphysics the smaller crystals within a parcel will sublimate away before the mean size crystal for that parcel would; indeed the mixing rates into that parcel for that period might be sufficient that the mean size crystal survives.

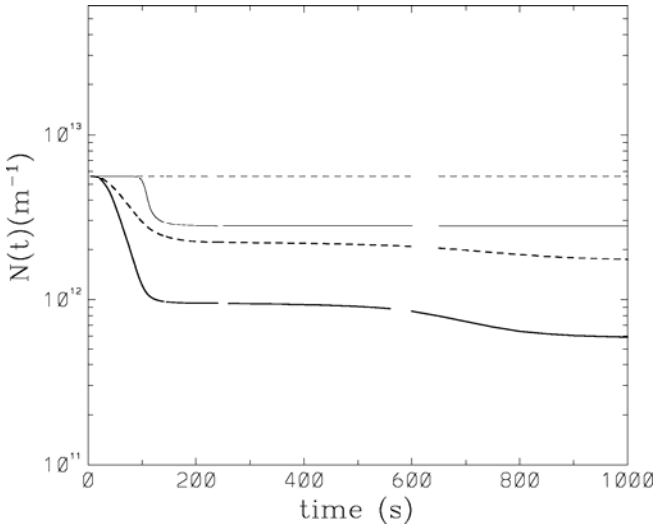

Figure 1. Changes in total ice crystal number as a function of time for B-767 at baseline conditions. Thin lines indicate bulk microphysics, thick lines binned microphysics. RH_i = 110% (solid lines) and RH_i = 130% (short dash).

The effects of RH_i were previously shown in Lewellen and Lewellen (2001) for the bulk model. With the binned microphysics, there is crystal loss due to adiabatic heating even for the higher RH_i value of 130%; the bulk model shows no crystal loss at this relative humidity level. As expected, the higher RH_i value produces less overall crystal loss and more total ice mass than the 110% case, but note that the crystal loss for the 130% binned case is greater than the 110% bulk case.

Figure 2 shows the cross-stream integrated drift plots of ice crystal number density for RH_i of 110% and 130%. The drift plot format was described by Lewellen, et al. (1998) and is inspired by scanning lidar measurements of wakes. The wake is sampled as if it were being advected at a steady rate by a mean wind aligned with the contrail. The horizontal axis in each case then varies over time as well as downstream distance, providing both temporal evolution and spatial structure. The 110% case loses a large portion of the bottom of the plume as compared to the130% case where a larger portion survives the descent of the vortices.

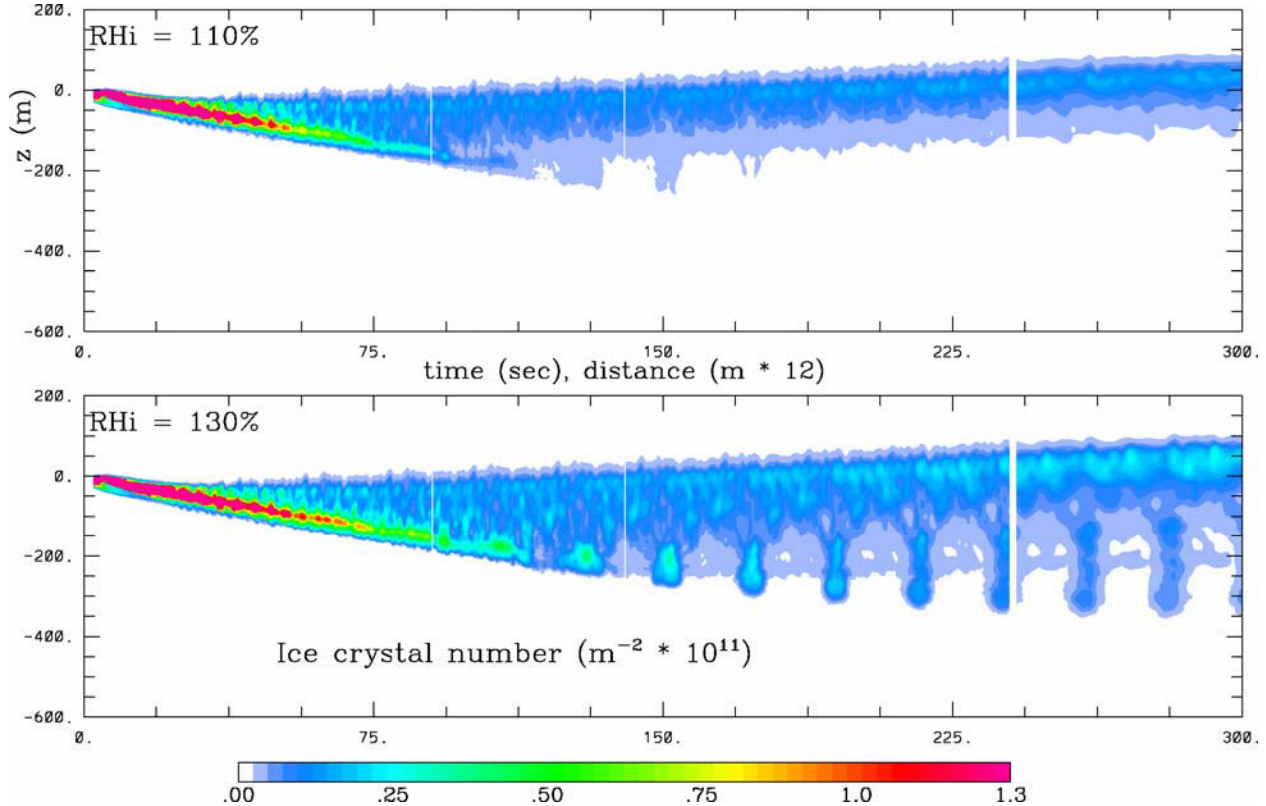

Figure 2. Drift plot of downstream space/time versus height of cross-stream integrated ice crystal number for B-767 contrail (binned microphysics) with RH_i = 110% (top) and 130% (bottom).

Figure 1 also has another point of interest with respect to the binned results. For both RH_i cases there is some late-time crystal loss which occurs well after the vortex system has died out. There is a buoyant "sloshing" of the wake plume that dominates the dispersion from the time of vortex demise (~200 s in the present case) out to ~2 Brunt-Väisälä periods. The bottom of the plume, which by 200 s has acquired significant positive buoyancy, buoyantly rises, overshoots its equilibrium level and then falls again. This second downward cycle (from ~500-800 s) is apparently the origin of the secondary crystal loss seen, again due to adiabatic heating of the descending parts of the plume. The Brunt-Väisälä oscillations can clearly be seen in Figure 3, showing results out to 1000 s. This second round of crystal loss requires a competition between different size crystals and therefore was not found in the earlier bulk microphysics study.

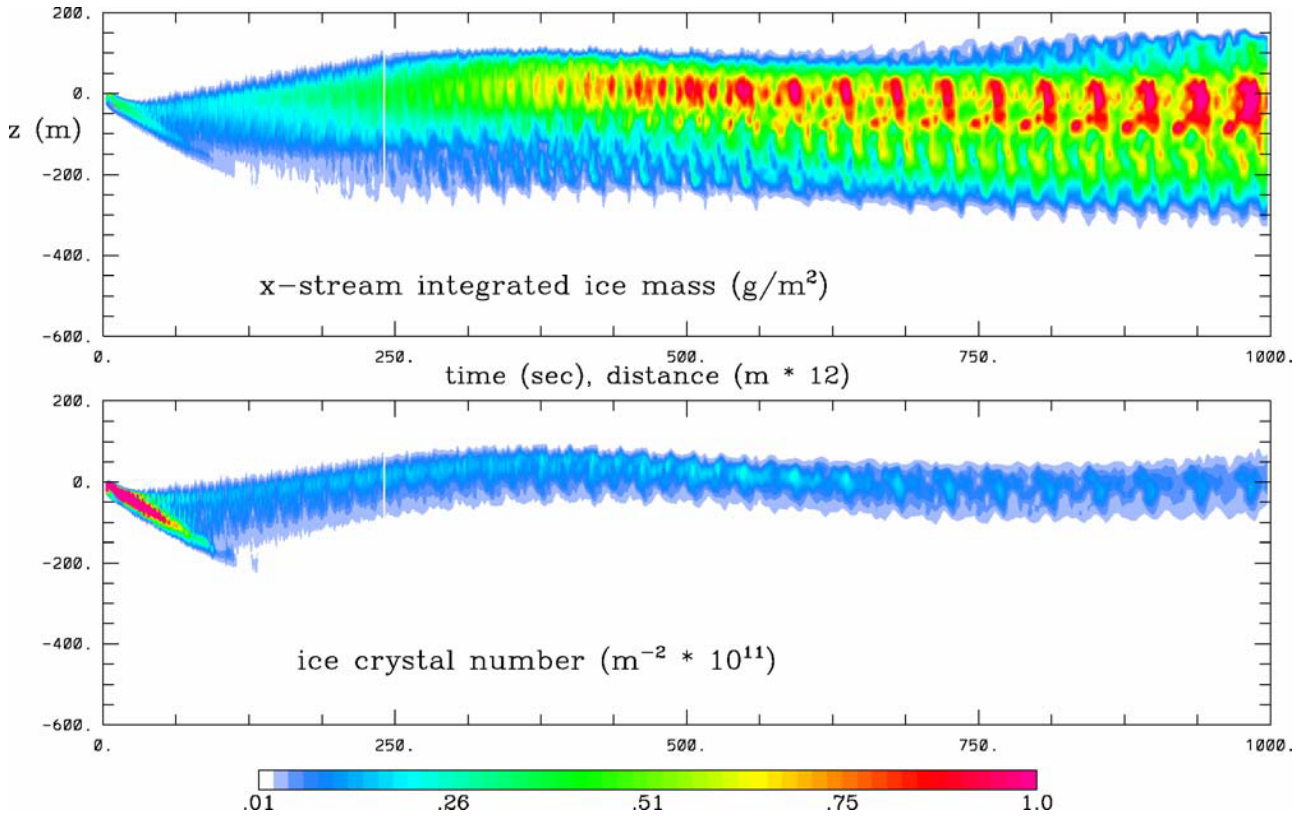

Figure 3. As in figure 2, but for B-767 at RH_i = 110% showing cross-stream integrated ice mass (top) and ice crystal number (bottom) out to 1000 s.

3.2 *Ice Binning and Initialization Choices*

Extensive studies were performed to ensure both proper initialization of the ice and proper selection of the binning parameters. Simulations showed that the contrail development was insensitive to the initial bin placement (within reasonable limits). The sensitivity to the uncertainty in the spatial distribution was tested and the results showed only modest changes to the contrail properties given sizable changes in distributions. Tests indicate that in cases similar to the present results, a bin mass ratio of 3.0 is likely the upper limit for adequate bin resolution. Simulations were also performed with a mass ratio of 2.5 which showed good agreement. The selection of the number of bins was based on the requirement that ice crystals do not pile up in the largest bin when atmospheric conditions dictate that continued growth is possible. The required number of ice bins ranged from 20 to 22, for RH_i of 110% and 130%, respectively, given a mass ratio of 3.0 and minimum radius of 50 nm; this corresponds to maximum crystal radii of 53 and 109 μm. At t = 1000 s, the use of these settings showed the largest two bins would either have no ice crystals or only be populated at a negligible level.

3.3 *Ambient Stratification*

For the baseline cases, the ambient potential temperature stratification was set to 2.5 *K/km*. Contrail simulations were also run with the stratification set to 1.0 and 10.0 *K/km*. In past work (Lewellen and Lewellen, 2001) it was found that increasing the stratification leads to an increase in detrain-

ment, a decrease in the vertical plume size (stratification fights against the drop of the vortices), and a dampening of the late-time buoyant sloshing. Figure 4 shows *N(t)* at the three different lapse rates with RH_i equal to 110%. The largest level of stratification has the greatest number of remaining ice crystals due to the decrease in total descent (~150 m compared to ~340 m), and hence less evaporation due to adiabatic heating. The figure also shows that the late-time crystal loss occurs earlier for the highest stratification level due to the reduced Brunt-Väisälä time scale.

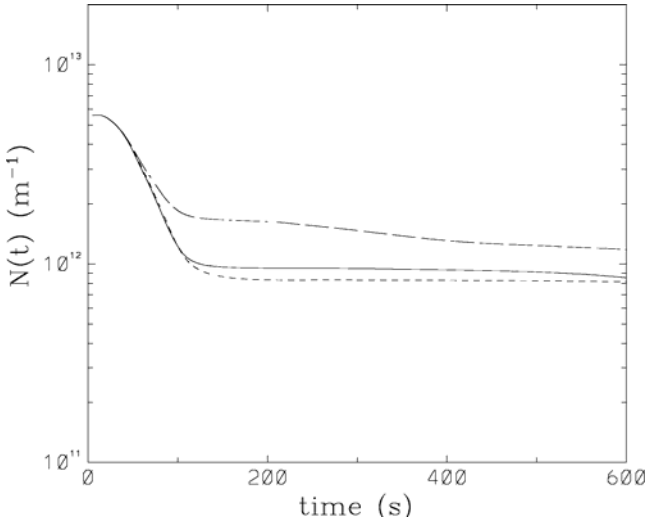

Figure 4. Effects of ambient stratification on contrail evolution for B-767 at RH_i = 110% with potential temperature gradients of 1.0 (short dash), 2.5 (solid line), and 10.0 *K/km* (long dash).

3.4 *Cross-Stream Wind Shear*

The cross-stream shear simulations apply a linear vertical wind shear (*du/dz*) that is perpendicular to the wake axis. Weak shear levels have little effect on the vortex dynamics. The primary difference comes in the appearance of the contrail since the cross-stream shear will horizontally smear the ice plume. Higher levels of cross-stream shear can significantly alter the baseline vortex dynamics. For the counter rotating vortex pair, one of the vortex cores will decay quicker since its vorticity has the opposite sign to that of the cross-stream shear vorticity, while the other vortex core will have its decay delayed. Even at high levels of cross-stream shear, the Crow instability can be the dominant decay mode for the vortex system, as long as the shear time scales are larger than the vortex dynamics time scales, which is the case for the shear levels considered here. Only modest differences are found in *N(t)* between the shear and no shear cases. The temporal evolution of the total ice mass shows a more dramatic difference (figure 5). The cross-stream shear case has a ~30% higher ice mass at 200 s (approximate end of vortex lifetime) than the non-shear case. These differences continue to grow at later times as the cross-stream shear leads to increased mixing with ambient supersaturated air.

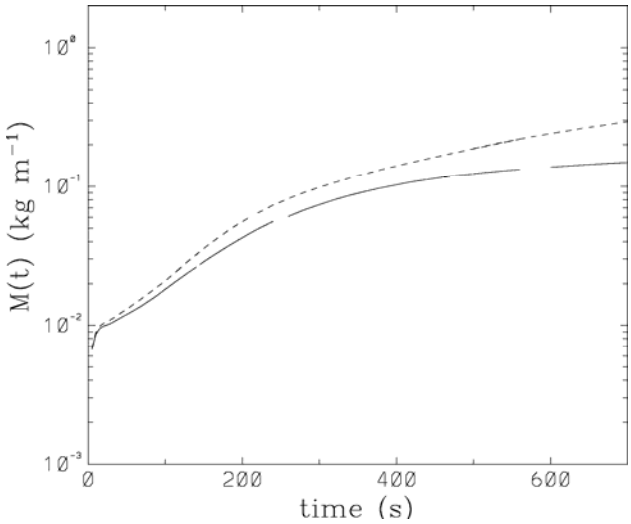

Figure 5. Effects of wind shear on total ice mass as a function of time for B-767 at RH_i = 110% with no shear (solid line) and cross-stream wind shear of 0.01/s (short dash).

3.5 *Aircraft Parameters*

A key aircraft parameter was also varied to investigate the effects on contrail evolution: assumed ice crystal emission index (EI_i). Simulations were conducted with EI_i an order of magnitude larger or smaller than the baseline value. Decreasing EI_i increases the average crystal size, causing a higher fraction of the crystals to survive. Thus an order of magnitude decrease in EI_i leads to a much less than order of magnitude decrease in $N(t)$ at late times. An increase in EI_i has the opposite effect; a larger fraction of ice crystals are lost to evaporation. Both trends are due to a competition for available moisture. Decreasing the number of initial crystals decreases the competition for moisture and hence a larger percentage of the crystals can grow large enough to survive the adiabatic heating phase. Increasing the number of initial crystals causes a greater competition for the moisture, which results in the ice crystals being more susceptible to evaporation. More work is needed to evaluate the sensitivity of these results to varying ambient conditions.

4 CONCLUSIONS

High-resolution LES has been coupled with binned ice microphysics to explore the sensitivity of contrail evolution to atmospheric and aircraft properties. There were significant differences seen with the binned microphysics as compared to the bulk model, primarily an overall difference in crystal loss, which will have a lasting impact on the late-time contrail properties such as radiative forcing. The simulations also demonstrated a previously undocumented late-time crystal loss that is only captured with a binned microphysics. The temperature stratification and wind shear results follow the trends shown in some past studies, but have now been obtained with LES using binned microphysics. Variation of the ice crystal emission index demonstrated the competing effects among crystal number, crystal size and the potential loss to evaporation. A more extensive sensitivity study varying aircraft type, EI_i, ambient pressure, temperature, humidity and wind shear and following the contrail development out to later times is ongoing and will be presented in future work.

ACKNOWLEDGMENTS

The authors would like to thank Steve Baughcum, Mikhail Danilin, Jeffrey Crouch and other colleagues at Boeing for their support and help in this work. The authors also thank Eric Jensen for initially providing us with the CARMA microphysics package.

REFERENCES

Jensen, E.J., A.S. Ackerman, D.E. Stevens, O.B. Toon, and P. Minnis, 1998: Spreading and growth of contrails in a sheared environment. *J. Geophys. Res. 103*, 31557-31567.

Lewellen, D.C. and W.S. Lewellen, 1996: Large-eddy simulations of the vortex-pair breakup in aircraft wakes. *AIAA J. 34*, 2337-2345.

Lewellen, D.C., W.S. Lewellen, L.R. Poole, R.J. DeCoursey, G.M. Hansen, and C.A. Hostetler, 1998: Large-eddy simulations and lidar measurements of vortex-pair breakup in aircraft wakes. *AIAA J.* 36, 1439-1445.

Lewellen, D.C. and W.S. Lewellen, 2001: The effects of aircraft wake dynamics on contrail development. *J. Atmos. Sci. 58*, 390-406.

Minnis, P., D. Young, L. Ngyuen, D. Garber, W. Smith, and R. Palikonda, 1998: Transformation of contrails into cirrus during SUCCESS. *Geophys. Res. Lett., 25*, 1157-1160.

Penner, J.E., D.H. Lister, D.J. Griggs, D.J. Dokken, and M. McFarland, 1999: *Aviation and the Global Atmosphere*, Cambridge Univ. Press, New York.

Spalart, P.R. and S.R. Allmaras, 1992: A one-equation turbulence model for aerodynamic flows. AIAA Paper 92-0439, 30th Aerospace Sciences Meeting and Exhibit.

Sussmann, R. and K.M. Gierens, 1999: Lidar and numerical studies on the different evolution of vortex pair and secondary wake in young contrails. *J. Geophys. Res. 104*, 2131-2142.

Global distribution of ship tracks from one year of AATSR-data

M. Schreier*, H. Bovensmann
Institute of Environmental Research, University of Bremen, 28359 Bremen, Germany

H. Mannstein, V. Eyring
DLR - Institut für Physik der Atmosphäre, Oberpfaffenhofen, 82234 Wessling, Germany

Keywords: ship tracks, radiative forcing

ABSTRACT: The perturbation of a cloud layer by ship-generated aerosol changes the cloud reflectivity and is identified by elongated structures in satellite images, known as ship tracks. As ship tracks indicate a pollution of the clean marine environment and also affect the radiation budget below and above the cloud, it is important to investigate their radiative and climate impact. In this study we use satellite data to examine the effects of ship tracks on a particular scene as well as on the global scale. The cloud optical and microphysical properties are derived using a semi-analytical retrieval technique combined with a look-up-table approach. Within the ship tracks a significant change in the droplet number concentration, the effective radius and the optical thickness are found compared to the unaffected cloud. The resulting cloud properties are used to calculate the radiation budget below and above the cloud. Local impacts are shown for a selected scene from MODIS on Terra. The mean reflectance at top of atmosphere (TOA) is increased by 40.8 Wm^{-2}. For a particular scene chosen close to the West Coast of North America on 10th February 2003, ship emissions increase the backscattered solar radiation at TOA by 2.0Wm^{-2}, corresponding to a negative radiative forcing (RF). A global distribution of ship tracks derived from one year of AATSR data shows high spatial and temporal variability with highest occurrence of ship tracks westward of North America and the southwest coast of Africa, but small RF on the global scale.

1 INTRODUCTION

Emissions from ships significantly contribute to the total budget of anthropogenic emissions. The principal exhaust gas emissions from ships include CO_2, NO_x, SO_x, CO, hydrocarbons, and particulate matter (Eyring et al., 2005). Compared to other transport modes, the sulphur content of the fuel burned in marine diesel engines and the total amount of SO_x emissions is high. The average sulphur fuel content of today's world-merchant shipping fleet is 2.4% resulting into a large amount of SO_2 and particulate matter emission totals (EPA, 2000).

The SO_2 and particle emissions from ships change the physical properties of low clouds. This is the so-called indirect aerosol-effect, which has been observed in satellite data in many studies (e.g., Conover, 1966; Twomey et al., 1968; Radke et al., 1989). The natural number of cloud condensation nuclei is limited and reflected in larger droplets and a smaller droplet number concentration in low-level stratiform clouds over the ocean compared to continental clouds. In case of injection of additional aerosols, the changes of the aerosol concentration and amount result in a change in the droplet number concentration within the cloud (Facchini et al., 1999), depending on the solubility and size of the injected aerosol particles. Particles and their precursors from ship emissions are able to act as cloud condensation nuclei (CCN) in the water vapour saturated environment of the maritime cloud or can change the surface tension due to the solubility. Especially the high sulphur content of the fuel may be an important factor for the modification of clouds, because the resulting SO_x is able to act as CCN. Amount and size of these particles depends on the fuel and also the kind of combustion, but can possibly result in a higher droplet concentration (Twomey et al., 1968;

* *Corresponding author:* Mathias Schreier, Institute of Environmental Research, University of Bremen, 28359 Bremen. Email: schreier@iup.physik.uni-bremen.de

Twomey, 1974) and consequently in a change of reflectivity of the maritime cloud. The increased reflectivity is even higher in the near infrared, because here, the ratio of absorption to scattering is strongly depending on the droplet size (Coakley et al., 1987; Kokhanovsky et al., 2004). In this study the modification of clouds and the influence of the ship exhaust on the radiation budget of a given scene are examined. Full details can be found in Schreier et al. (2006) and only a brief summary is presented here. Satellite data are also used to retrieve cloud properties and their modifications due to ship emissions on the global scale.

2 METHODS

2.1 *Cloud properties retrieval*

A new algorithm has been developed that combines the semi-analytical cloud retrieval algorithm SACURA (Kokhanovsky et al., 2003) and look-up-tables (LUTs) for thin clouds calculated with the libRadtran radiative transfer package (Mayer and Kylling, 2005). An advantage of the new algorithm is that it can be applied to different satellite instruments with channels in the near infrared (e.g. Terra-MODIS, AATSR).

The optical and microphysical parameters of the cloud were derived from the 0.9 μm and 1.6 μm channels for MODIS and AATSR. 1.6 μm was selected because the smaller absorption of liquid water enables more accurate results for the SACURA-retrieval. The two cloud retrieval algorithms - SACURA and LUTs - are different, but both derive the cloud optical thickness and also the effective radius r_{eff}, defined by the ratio of the third to second moment of the particle size distribution and therefore indicating a change of the ratio of volume to surface in the particle size distribution.

The columnar droplet number concentration for both retrievals is calculated via effective radius and cloud optical thickness by assuming a gamma droplet size distribution with a coefficient of variance of 0.37. Calculations of droplets per volume (N) were performed using a hypothetical vertical homogeneous cloud of a thickness 500 m, which is a reasonable value for low marine stratiform clouds.

2.2 *Estimating impact on the radiation field*

The derived optical parameters were used to estimate changes in solar radiation for the areas below and above the cloud as well as the thermal outgoing radiation by radiative transfer calculations. Optical thickness and the effective radius have been applied to create look-up-tables for the solar flux via the radiative transfer code libRadtran (Mayer and Kylling, 2005), by using the built in k-distribution by Kato et al. (1999) to calculate integrated solar irradiance with the solver disort2 (Stamnes et al., 1988) for the wavelength range of 0.24 μm to 4.6 μm. The down-welling irradiance at the surface and the up-welling flux at TOA were calculated for the mid-latitude winter atmosphere. The different distributions of cloud optical properties were considered by using these look-up-tables to calculate the solar flux for every pixel and taking into account the local solar zenith angle. The cloud top height was chosen to be 1000 m and the cloud-bottom height was 500 m. The optical properties of the clouds were calculated according to Mie theory. The mean values for all low-cloud-pixels, ship-track-pixels and no-track-pixels were determined, to estimate the impact of ship tracks on both, the solar radiation at the surface and the backscattered radiation at TOA.

3 ANALYSIS OF SHIP A TRACK SCENE

A particular and adequate satellite scene from Terra-MODIS (King et al., 1995) was selected to show local impacts. The scene from 10th February 2003, close to the West Coast of North America (153°W to 120°W and 40° N to 60° N), exhibits a number of anomalous cloud lines in the stratiform clouds over the ocean.

3.1 *Cloud properties*

The cloud retrieval algorithm (section 2) was used to calculate optical and microphysical parameters of low clouds (Fig. 1). A significant decrease of the average effective radius from 12 μm to 6

µm is visible across the ship-track-pixels (Fig. 1a). The optical thickness of unpolluted clouds is about 20 to 30 and is increasing in the track up to 45 and higher (Fig. 1b). Also the change in the droplet number concentration from around 100 cm^{-3} up to 800 cm^{-3} is substantial (Fig. 1c). Table 1 summarizes the mean values of the various parameters for all low-cloud-pixels, ship-track-pixels and no-ship-track-pixels. The decrease in the effective radius from 13.2 to 10.1 µm for the area is evident and also an increase in cloud optical thickness from 20.7 up to 34.6 is observed. There is also an obvious increase of droplet number concentration from 79 to 210 cm^{-3}.

Table 1. Mean values of cloud parameters for all low-cloud-pixels, ship-track-pixels and no-ship-track-pixels..

	Low-cloud-pixels	No-ship-track-pixels	Ship-track-pixels
Effective radius (µm)	13.0	13.2	10.1
Optical thickness	21.4	20.7	34.6
Droplet number (cm^{-3})	85	79	210

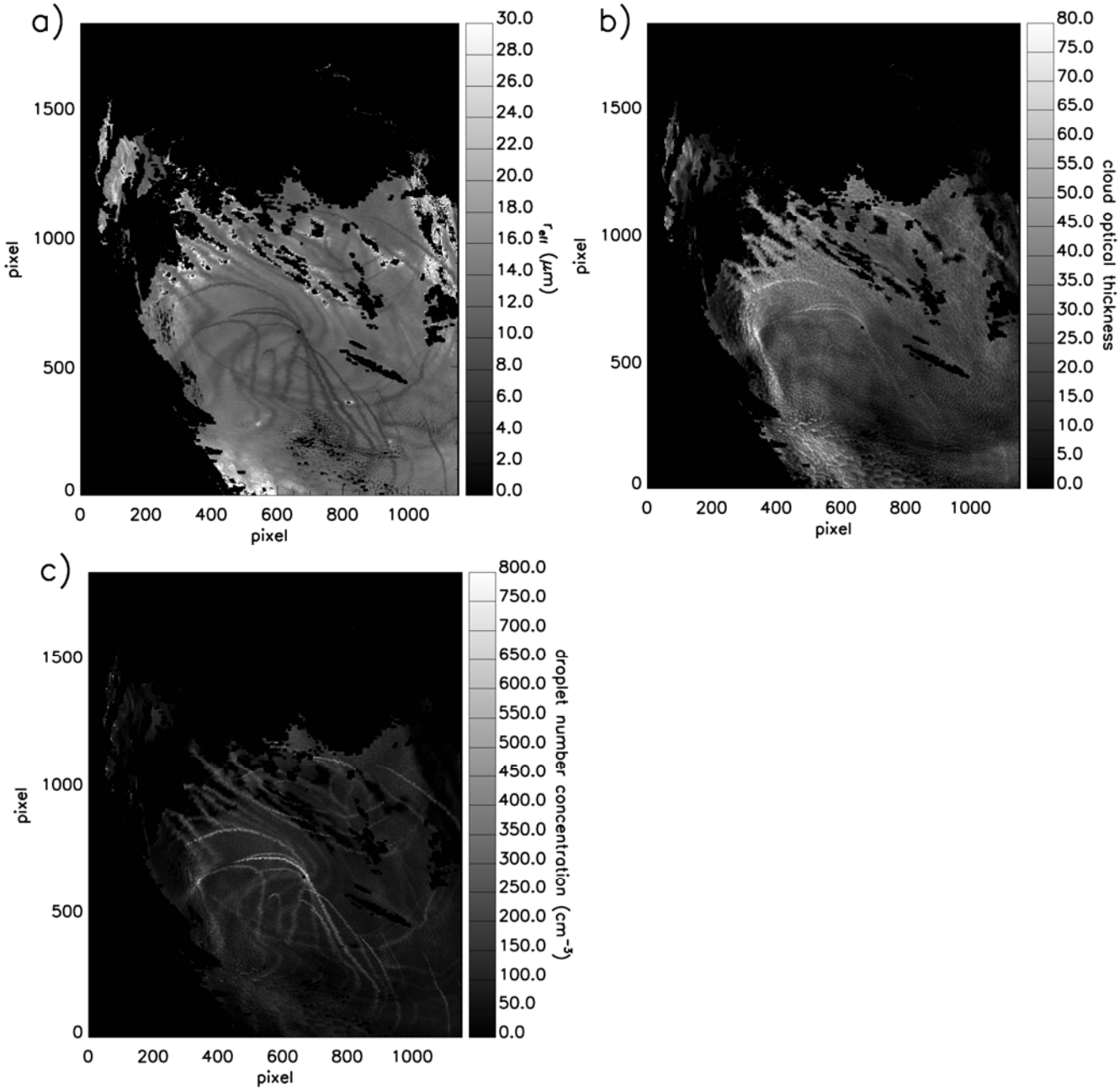

Figure 1: Effective radius (a), cloud optical thickness (b) and concentration of particles (c) (cm−3) derived from the MODIS channels 2 and 6 for the analysed scene. From Schreier et al. (2006).

3.2 *Radiative Effects*

To separate the impact of changes in cloud parameters from ship tracks on the radiation field without the uncertainties represented by the solar zenith angle variations, radiative transfer calculations were performed assuming a mean solar zenith angle of 63° for all pixels. The calculated values now only depend on the cloud optical properties, as the influence of a varying solar zenith angle has been eliminated.

Assuming a constant solar zenith angle, at TOA, ship-track-pixels reflect 40.8Wm^{-2} more than the no-ship-track-pixels. The amount of ship-track-pixels in the scene is 6.7%. The net radiative effect of the change in cloud properties due to ships for the particular scene is estimated by calculating the difference of the absolute radiation values between all low-cloud-pixels ($E_{low-cloud}$) and the no-ship-track-pixels ($E_{no-ship-track}$). According to these values, the solar radiation at the surface is reduced on average by 2.1Wm^{-2} by the ship emissions and additional 2.0Wm^{-2} are reflected back at TOA.

4 GLOBAL DISTRIBUTION OF SHIP TRACKS

The global distribution of ship tracks is derived from data of the AATSR (Advanced Along Track Scanning Radiometer) instrument aboard the European ENVISAT satellite for the year 2004.

To select scenes dominated by low clouds over ocean, we applied the following criteria: (1) excluding clouds over land via the terrain height, (2) distinguish between ocean and clouds by the reflectance of a channel in the short wavelength and (3) estimation of cloud top height with the help of the 11μm channel. The remaining scenes include 'very low clouds', which were further examined and the scenes that included ship tracks were used to estimate the global coverage of ship tracks with a resolution similar to the International Cloud and Climate Project was calculated.

The results show highest occurrence of ship-tracks over the Northern Pacific and the Northern Atlantic (up to 0.2%). A comparable high amount of ship-tracks is also found at the Western Coast of Africa and in the Northern Atlantic. In addition to large regional variations, large seasonal variations have been found, with most ship-tracks occurring in springtime and in summer, and only few in wintertime and autumn.

Calculation of the increased backscattering compared to the surrounding for fixed solar zenith angle show most values are around 40Wm^{-2}. This indicates an increased cooling of the atmosphere on regional scale. On global scale, the estimations for radiative forcings show values smaller than -1 mWm^{-2}, which is small compared to other radiative forcings.

5 CONCLUSIONS

On the basis of a particular satellite scene it has been shown that ship emissions modify existing clouds on a regional scale by decreasing the effective radius, while they increase droplet concentration and optical thickness (Schreier et al., 2006). The results agree with the theory and experiment (Öström et al., 2000; Hobbs et al., 2000): Low clouds of the maritime boundary layer have less cloud condensation nuclei than clouds over land; in consequence, this results in larger droplet radii for similar water content and dispersion of droplet size distributions. Injection of aerosols and their pre-cursors by ships results in more CCNs causing the mean droplet radius to decrease and the droplet number concentration to increase. The derived parameters were used to calculate changes in the radiative energy budget below and above the cloud. The mean values show an increase of 40.8Wm^{-2} at TOA. If the whole low-cloud area with 6.7% ship-track-pixels is taken into account, an increase of 2.0Wm^{-2} in backscattered solar radiation was found, when assuming a constant solar zenith angle of 63° for the scene. Full details of this study can be found in Schreier et al. (2006).

The global distribution of ship tracks shows high occurrence over the Northern Pacific and the West Coast of Africa. A first estimate of the global impact of ship tracks result in only small radiative forcings compared to other ship-induced RFs. However, due to large seasonal and spatial variations ship tracks can impact the climate locally.

REFERENCES

Coakley Jr., J.A., P.A. Durkee, K. Nielsen, J.P. Taylor, S. Platnick, B.A. Albrecht, D. Babb, F.L. Chang, W.R. Tahnk, C.S. Bretherton, P.V. Hobbs, 2000: The Appearance and Disappearance of Ship Tracks an Large Spatial Scales, *J. Atmos. Sci.*, 57 , 2765-2778.

Conover, J.H., 1966: Anomalous Cloud Lines, J. Atmos. Sci., 23, 778-785.

EPA, 2000: United States Environmental Protection Agency Air and Radiation, Analysis of Commercial Marine Vessels Emissions and Fuel , *EPA420-R-00-002*.

Eyring, V., H.W. Köhler, J. van Aardenne, and A. Lauer, 2005: Emissions from international shipping: 1. The last 50 years, *J. Geophys. Res.*, 110, D17305.

Facchini, M.C., M. Mircea, S. Fuzzi, R.J. Charlson, 1999: Cloud albedo enhancement by surface-active organic solutes in growing droplets, *Nature*, 401, 257-259.

Hobbs, P.V., T.J. Garrett, R.J. Ferek, S.R. Strader, D.A. Hegg, G.M. Frick, W.A. Hoppel, R.F. Gasparovic, L.M. Russell, D.W. Johnson, C. O´Dowd, P.A. Durkee, K.E. Nielsen, G. Innis, 2000: Emissions from Ships with their respect to clouds, *J. Atmos. Sci.*, 57, 2570-2590

Kato, S., T.P.Ackermann, J.H. Mather, E.E. Clothiaux, 1999: The k-distribution method and correlated-k approximation for a shortwave radiative transfer model, *J. Quant. Spectrosc. Radiat. Trans.*, 62, 109-121.

Kokhanovsky, A.A., V.V. Rozanov, E.P. Zege, H. Bovensmann, J.P. Burrows,2003: A semi-analytical cloud retrieval algorithm using backscattered radiation in 0.4-2.4 micrometers spectral range, *J. Geophys. Res.*, 108(D1), 4008.

Kokhanovsky, A., 2004: Optical properties of terrestrial clouds, *Earth Science Reviews*, 64, 189-241.

Mayer, B., A. Kylling, 2005: Technical note: The libRadtran software package for radiative transfer calculations, description and examples of use, *Atmos. Chem. Phys.*, 5, 1855-1877.

Öström, E., K.J. Noone, R.A. Pockalny, 2000: Cloud Droplet Residual Particle Microphysics in Marine Stratocumulus Clouds Observed during the Monterey Area Ship Track Experiment, *J. Atmos. Sci.*, 57, 2671-2683.

Radke, L.F., J.A. Coakley Jr., M.D. King, 1989: Direct and Remote Sensing Observations of the Effects of Ships on Clouds, *Science*, 346, 1146-1149.

Schreier, M., A. A. Kokhanovsky, V. Eyring, L. Bugliaro, H. Mannstein, B. Mayer, H. Bovensmann, and J. P. Burrows, 2006: Impact of ship emissions on the microphysical, optical and radiative properties of marine stratus: a case study, *Atmos. Chem. Phys.*, accepted.

Stamnes, K., S.C. Tsay, W. Wiscombe, K. Jayaweera, 1988: Numerically stable algorithm for discrete-ordinate-method radiative transfer in multiple scatteringand emitting layered media, *Appl. Opt.*, 27, 2502-2509.

Twomey, S., H.B. Howell, T.A. Wojciechowski, 1968: Comments on Anomalous cloud lines, J. Atmos. Sci., 25, 333-334.

Twomey, S., 1974: Pollution and the planetary albedo, *Atmosph. Environ.*, 8, 1251-1256.

Assessment of a Global Contrail Modelling Method

K. Klima*, I. Waitz
MIT, Cambridge, Massachusetts, USA

Keywords: contrail, contrails, aviation, contrail modelling, SAGE, RHi, satellite images, aircraft tracts, radar based trajectory, cloud formations, linear features, CONUS, RUC

ABSTRACT: Estimates of radiative forcing contributions from aircraft have raised concerns about the impacts of contrails and aviation-induced cirrus on climate. Increasing demand for aviation will further increase the incidence of contrails. This paper describes the assessment of a method for estimating the formation of contrails. The method couples radar-based flight trajectory information with hourly meteorological data. Estimates of persistent contrails were compared to results obtained from NASA satellite images. For the one week time period we considered, the contrail model coupled with measured aircraft flights tracks did not accurately estimate the occurrence of persistent contrails. This was due both to a limited ability to identify contrails in the satellite images (as a basis for validating the methods) and to uncertainties in the meteorological data and the contrail modeling methods.

1 INTRODUCTION

Estimates of radiative forcing contributions from aircraft have raised concerns about the impacts of contrails and aviation-induced cirrus on climate (IPCC 1999). Within four to six hours after initial formation, contrails, if they persist, may evolve into aviation-induced cirrus. In a study of one region in Europe, contrails were estimated to produce a local annual mean radiative forcing of 0.23 W/m^2 (Stuber et al., 2006). The global and annual average forcing was recently estimated to be 0.01 W/m^2 (Sausen et al., 2005).

There are currently only limited capabilities for evaluating the extent and effects of global contrail coverage. Examples of other work in this area include Williams et al. (2005) who analyzed fuel burn and carbon dioxide penalties as a function of contrail reduction, and Minnis et al. (2004), who described a method to calculate whether a contrail will form and persist along certain routes. Both of these studies used the Appleman criteria (1953) to determine whether or not a contrail will form and persist, and the method presented by Schumann (2000) to relate the thermodynamic conditions in the aircraft plume to the overall propulsive efficiency. Duda et al. (2005) improved upon Minnis's method by using flight data to compute air traffic density. A recent paper by Mannstein, Spichtinger, & Gierens (2005) studied high resolution vertical radiosonde meteorological data, and calculated the potential reduction of contrails by a small change in flight altitude (0 to 1000ft).

This paper presents the assessment of a method for estimating contrail formation and persistence. The method couples radar-based flight trajectories with assimilated meteorological data. The method is assessed through a direct comparison of contrail estimates to satellite imagery.

2 NUMERICAL MODEL

2.1 *Aviation System Model*

To estimate contrail formation, an aircraft model is needed to estimate aircraft overall propulsive efficiency and the emissions index of water. Note that contrail formation does not change greatly as a function of fuel burn (being more significantly influenced by local atmospheric conditions). How-

* *Corresponding author:* Kelly Klima, MIT, 54-1719, 77 Massachusetts Ave, Cambridge, MA, USA. Email: klima@mit.edu

ever, an accurate aviation system model is needed to examine the extent of contrail coverage. This study used the fuel burn and emissions module of the FAA's System for assessing Aviation's Global Emissions (Kim et al. 2006a, Kim et al. 2006b).

SAGE accepts flight tracks from Enhanced Traffic Management System (ETMS) radar data and therefore contains detailed temporal and spatial information for most of the flights over the continental United States. These flights are processed through the SAGE model, which consists of individual modules (e.g. aerodynamics, engine thrust, etc.) that interact to create a fuel burn estimate. SAGE can therefore calculate the overall propulsive efficiency of each aircraft along the flight trajectory. For the purposes of this research, we examined 54,000 United States continental flights. Sensitivity to aircraft performance modelling was addressed and is discussed in Klima, (2005).

2.2 *Meteorological Data*

The Rapid Update Cycle (RUC) is an atmospheric prediction system comprised primarily of a numerical forecast model and an analysis system to initialize that model ([http://ruc.noaa.gov]). The RUC has been developed to serve users needing short-range weather forecasts. RUC runs operationally at the National Centers for Environmental Prediction (NCEP). Archived RUC data were obtained from a United States program called the Atmospheric Radiation Measurement Program (ARM, [http://www.arm.gov/]) for dates November 12-18, 2001 (to match available satellite imagery/contrail mask data) and October 2000 (to match available fuel burn data). This study used 40km resolution data so that its output could be compared to that of NASA Langley (Duda 2003, Minnis 2004). See Klima (2005) for implementation details.

Satellite data were provided by NASA Langley for the hours of 17-24 Universal Time Conversion (UTC) for the week of November 12-18, 2001. One set of data were satellite infrared radiances (IR) from the Sun-synchronous NOAA-16 Advanced Very High Resolution Radiometer (AVHRR) 1-km imager, 10.8 & 12 μm bands (Figure 1, right). Another set of data were contrail masks (Figure 1, left). The satellite data sets for deriving the contrail coverage consist of the NOAA-16 data and multispectral 1-km data from the MODerate Resolution Imaging Spectroradiometer (MODIS) on the Terra satellite (Duda, 2003). NASA Langley researchers applied Mannstein's algorithm (1999) to identify contrails in the satellite imagery. Filtering methods were provided by NASA Langley, and consist of removing points a) outside the satellite image range, and b) near the edges of the image where curvature is high (scan angle magnitude is more than 50°).

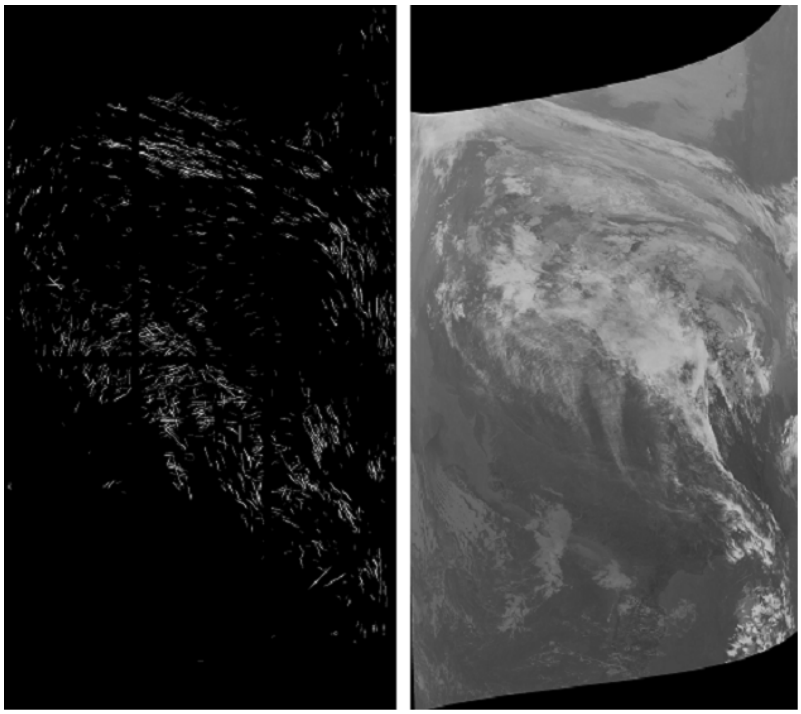

Figure 1 - NOAA-16 satellite image (left) and matching contrail mask (right, white pixel indicates contrail formation), November 18, 2001 1888 UTC. Note that the satellite image is reversed from east to west. This occurs due to the direction the satellite passes overhead.

2.3 *Contrail Model*

The aircraft type-specific emissions index of water and the type-specific engine efficiency are reported by SAGE along each chord of the radar trajectory. Then, the temporally and spatially matching relative humidity for ice (RHi) is obtained from the meteorological data sets. The method used to estimate the formation of contrails is based on the methods of Appleman (1953) and Schumann (2000).

We implemented this model using an empirical saturation curve (Sonntag, 1994) and the derived mass-averaged moist air specific heat (Klima, 2005). Given gridded meteorological conditions, aircraft fuel burn, aircraft engine overall efficiency, and fuel characteristics, this model can be used to calculate whether a contrail will form or persist at each location in along the flight path. It reports contrail formation as percentage of distance traveled, and differentiates between contrails forming in clouds and in clear skies (if RHi >75%, the area is assumed to be a cloud). A first-order advection model is applied to the contrails to account for their change in location over time.

Due to the complexity of contrails (see for example, Atlas et al., 2006), several characteristics were not addressed. First, we did not estimate the time evolution of the shapes/sizes of contrails. Second, we did not address sub-grid scale variability in meteorological data. Third, optical depth and radiative forcing were not addressed in this study. Fourth, overlapping contrails were ignored due to the small average width of contrails (satellite images indicate less than 10km) and the small regions of ice-supersaturation. Fifth, we assumed winds are invariant from time of contrail formation. Sixth, the evolution of contrails into aviation-induced cirrus cloudiness was beyond the scope of this study. Finally, the environmental effect of contrails was not addressed.

3 RESULTS

Since contrail identification is integral to comparison of actual and model-predicted contrails, a brief description of the contrail identification method is necessary. Young contrails have a smaller crystal size than natural clouds, and hence have a higher IR transmissivity (brightness) in the 10.8μm image as compared to the 12μm image. Hence a brightness-differencing scheme can be used to identify all image pixels which may be contrails: the 10.8μm minus 12μm brightness temperature difference. However, using only a temperature differencing technique could identify singular pixels, edges of clouds, or ground features. A second property of contrails is their linear structure, especially at a young age. Hence a linear filter is used. Extended information on processing techniques is described by Mannstein et al. (1999).

There is only limited confidence in the ability of these techniques to identify contrails. Wind shear, turbulence and ice particle sizes will affect how the contrail grows and disperses. Young contrails (less than about 50 minutes) and weak contrails are too small to be sensed by the satellites, and therefore are typically not identified. Older contrails (greater than 2.5 hours) have begun to lose their linear features, and so would also not be identified with confidence (Duda, 2003).

NASA Langley estimate the false alarm rate for identification of contrails using these methods is 40% (Minnis, 2004). For example, for the satellite images we examined, many of the features identified as contrails were oriented north-south. Over the continental United States, most of the air traffic is east-west. Since an aircraft is necessary for contrail formation, these were probably false alarms. In particular, striated cirrus cloud formations were often misidentified as contrails.

3.1 *Comparison of Contrail Mask to RHi fields*

Theoretically, clouds and/or contrails should sublime at RHi < 100%. Visual comparison of the contrail masks to satellite data showed that the linear features with high brightness differences were usually either contrails or clouds; they were rarely associated with ground features. Consequently, an accurate RHi data set would be expected to have RHi > 100% in most areas identified as contrails (whether these areas corresponded to contrails or striated cirrus cloud formations). Contrail mask data from the satellite images and modeled contrail estimates were transferred into specific latitude and longitude points. Next these figures were overlayed on RHi images. Figure 2a shows the contrail mask data on November 12, 2001 at 1996 hours, universal time. Note that this figure is filtered to contain only the region of data present in the satellite image (filter denoted by crosses).

Visual examination of Figure 2a shows that contrail pixels appear in areas of RHi < 100%. Similar results were obtained for the other days examined. We then calculated the fraction of contrail mask pixels that would appear in the CONUS region (at 10973m, 36000ft altitude) given a variable RHi threshold. Based on this calculation, we determined that roughly 60-90% of the contrail pixels were misidentified. This result reflects the inability of the meteorological model to predict supersaturation. This exercise demonstrates that the RHi fields, although perhaps representative of the large scale features, did not accurately capture the atmospheric conditions on the days we examined.

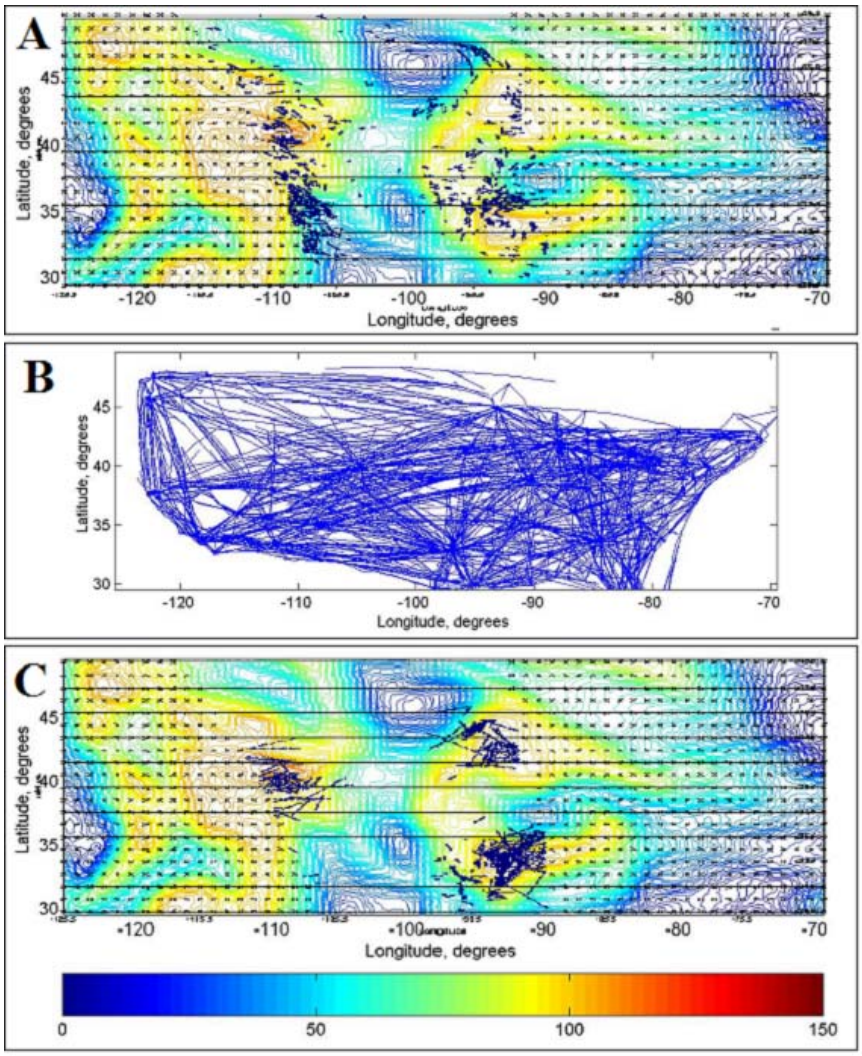

Figure 2 – 11/12/2001 hr 1996, RHi hour 19 field A) Filtered contrail mask. Contrails (47N 100W) caused by incorrect RHi field (temporally changing). Contrails (32N 110W) caused by threading B) Flights examined C) Filtered contrail estimation.

3.2 *Comparison of contrail model and satellite image mask results*

Comparisons were made for 53,844 U.S. continental flights performed during the week of November 11/12-18, 2001. Figure 2b shows the set of continental flights that temporally match the contrail mask image. Areas of contrail formation are generally consistent between the satellite images and the model estimates (see Figure 2a and Figure 2c). Where the images are not consistent, the estimated contrails match well with areas of high RHi in the meteorological data. The discrepancies can be attributed to the following reasons:

- Inability to represent RHi gradients with altitude – In the figure we overlay the contrail estimates (from throughout the atmosphere) on meteorological data from one altitude level.
- Incorrect RHi fields – The RHi fields in the meterological data are imperfect reconstructions of the true RHi fields.
- Misidentification of striated clouds and ground features as contrails. There are also regions where the clouds are so thick that contrails are not identified.

- Incorrect contrail advection – A shearing of contrails will appear due to a combination of aircraft traveling the same route and wind advection; a better contrail advection model may more correctly locate these contrails. Wind shear, turbulence, contrail precipitation, and stratification will all be important in determining how a contrail evolves.
- Insufficient flight data – Recall that this study examined commercial, continental U.S. flights only. Neglecting international flights leads to an underestimate of persistent contrails near the edges of the United States. This discrepancy does not apply to our example figures, but was noted in other results shown in Klima (2005).

3.3 *Contrail Persistence Threshold*

One important parameter in the contrail model is the percent of RHi at which contrails persist. For homogeneous nucleation of cirrus clouds, this threshold percent is thought to be 140-160% (Minnis 2004). However, contrails are formed primarily through heterogeneous nucleation. In the literature, the threshold is variously placed at somewhere between 95-105% (Duda 2003). The nominal value used in our study was 100%.

The effect of changing the contrail persistence threshold over the globe was examined. Assuming the RHi data were flawed and the contrail persistence threshold varied from 90-110% RHi (instead of the assumed 100% RHi), one can calculate the change in ground coverage over which contrails could form. Based on this analysis, if the contrail persistence threshold was allowed to vary from 90-110%, contrail coverage area could vary between 13%166% of the currently estimated coverage area. If the persistence threshold was allowed to vary as literature suggests from 95-105% RHi (instead of 100% RHi), continental coverage area could vary between 51%-135% of the currently estimated coverage area.

3.4 *Contrail Length*

The typical length of the estimated contrails was larger than 100km, (several degrees in length), while the typical length of the observed contrails was about 50km. This length is much larger than the meteorological grid scale resolution, so it is not a reflection of subscale RHi gradients.

This occurs because the SAGE model uses preprocessed ETMS data; in order to shorten the dataset for storage purposes, “chords” are constructed on which the aircraft travels the same direction and magnitude for a long period of time. The discrepancy between the long predicted contrails and the short contrails observed in the satellite images implies that the chord lengths used within SAGE need to be shortened - at least to the extent to where they are consistent with length-scales observed in the RHi data.

4 DISCUSSION

In this paper, we compared estimates of persistent contrails developed using radar-based flight trajectories and assimilated meteorological data to contrails identified from satellite data. This comparison highlighted the following issues.

First, it was not possible to match particular contrails observed in the satellite images to specific flight trajectories. This occurred largely because the contrail mask algorithm identified both contrails and striated cirrus cloud formations, suggesting limitations in the satellite sensing and extraction methods (Mannstein 1999). We estimate that perhaps 40-50% of the contrail pixels were misidentified.

Second, RUC RHi fields did not accurately portray the true RHi fields for the days examined in 2001. We found that 60-90% of the pixels identified as linear features (demonstrated to be contrails or clouds) were located in areas where the RHi estimated by the RUC meteorological model was theoretically too low to support clouds or contrails. The RUC models do not have the resolution or the microphysics to represent the small scale vertical motions thought to be important for predicting cirrus and thus RHi correctly. Hence at this point in time, it is unknown to what degree a contrail model coupled with measured aircraft flight tracks can be used to accurately estimate contrail formation as given by satellite images/contrail masks. Both the identification of contrails from satellite images and the estimation of upper atmospheric humidity are lacking.

Third, the typical length of the estimated contrails was larger than 100km, (several degrees in length), while the typical length of the observed contrails was about 50km. This length is much larger than the meteorological grid scale resolution, so is not a reflection of subscale RHi gradients. Rather, this occurs because the SAGE aviation model shortens the ETMS dataset for storage purposes. The discrepancy between the long predicted contrails and the short actual contrails implies that the chord lengths used within SAGE need to be shortened until they are consistent with length-scales observed in the RHi data.

These results are not necessarily general. We assessed only one week's worth of flights over the continental United States.

ACKNOWLEDGEMENT

This work was supported by the U.S. Federal Aviation Administration Office of Environment and Energy. Maryalice Locke and Mohan Gupta managed the project. We thank them for their guidance and contributions. We also thank Lourdes Maurice, Curtis Holsclaw and Carl Burleson of the FAA for their guidance and support. The work was the result of a long-standing collaboration with the Volpe National Transportation Systems Center and we thank Gregg Fleming, Brian Kim, Sathya Balasubramanian, Andrew Malwitz and Matt Maki for their contributions with the aviation system model, SAGE. We also thank Patrick Minnis, David Duda and Rabi Palikonda of NASA Langley Research Center for providing the satellite images and for their help interpreting them.

REFERENCES

Appleman, H., 1953: The Formation of Exhaust Condensation Trails by Jet Aircraft. *Bulletin American Meteorological Society 34*, 14-20.

Atlas, D., Z. Wang, D. Duda, 2006: Contrails to Cirrus – Morphology, Microphysics, and Radiative Properties. *Journal of Applied Meteorology and Climatology 45,* 5-19.

Duda, D.P., P. Minnis, P.K. Costulis, R. Palikonda, 2003: *CONUS Contrail Frequency Estimated from RUC and Flight Track Data.* European Conference on Aviation, Atmosphere, and Climate.

Kim, B., G. Fleming, S. Balasubramanian, A. Malwitz, J. Lee, J. Ruggiero, 2006a: *SAGE: Version 1.5 Technical Manual*. FAA-EE-2005-01 (http://www.faa.gov/about/office_org/headquarters_offices/aep/models/sage/)

Kim, B., G. Fleming, S. Balasubramanian, A. Malwitz, J. Lee, J. Ruggiero, 2006b: *SAGE: Version 1.5 Technical Manual*. FAA-EE-2005-04 (http://www.faa.gov/about/office org/headquarters offices/aep/models/sage/).

Intergovernmental Panel on Climate Change. Aviation and the Global Atmosphere. Cambridge University Press: USA, 1999.

Klima, Kelly. Assessment of a Global Contrail Modeling Method and Operationsl Strategies for Contrail Mitigation. MIT: Boston, MA, 2005.

Mannstein, H., R. Meyer, P. Wendling, 1999: Operational detection of contrails from NOAA-AVHRR-data. *International Journal of Remote Sensing 20,* 1641-1660.

Mannstein, H., P. Spichtinger, K. Gierens, 2005: A Note on Avoiding Contrail Cirrus. *Transportation Research Part D 10*, 421-426.

Minnis, P., J.K. Ayers, R. Palikonda, E. Phan, 2004: Contrails, Cirrus Trends, and Climate. *Journal of Climate 17,* 1671-1685.

Sausen, R. I. Isaksen, V. Grewe, D. Hauglustaine, D. Lee, G. Myhre, M. Köhler, G. Pitari, U. Schumann, F. Stordal, C. Zerefos, 2005: Aviation radiative forcing in 2000: An update on IPCC (1999). *Meteorologische Zeitschrift 14-4*, 555-561(7).

Schumann, U., 2000: Influence of Propulsion Efficiency on Contrail Formation. *Aersp. Sci. Technol 4,* .391-401.

Sonntag, 1994: Advancements in the Field of Hygrometry. *Meteorol Zeit 3,* 51-66.

Stuber, N., P. Forster, G. Rädel, K. Shine, 2006: The importance of the diurnal and annual cycle of air traffic for contrail radiative forcing. *Nature 441,* 864-867.

Williams, V., R. Noland, R. Toumi, 2005. "Variability of contrail formation conditions and the implications for polices to reduce the climate impacts of aviation". *Transportation Research Part D* 12, 269-280.

Probabilistic Forecast of Contrails within Cirrus Coverage

D. P. Duda*
National Institute of Aerospace, Hampton, VA, USA

R. Palikonda
Analytical Services and Materials, Inc., Hampton, VA, USA

P. Minnis
NASA Langley Research Center, Hampton, VA, USA

Keywords: contrails, cirrus, forecasting

ABSTRACT: Meteorological variables derived from high-resolution numerical weather analysis models (Rapid Update Cycle (RUC) and Advanced Regional Prediction System (ARPS)) are compared with cirrus and contrail cloud occurrence deduced from multi-spectral radiances measured by the Advanced Very High Resolution Radiometer (AVHRR) onboard the NOAA-16 polar-orbiting satellite between April 2004 and June 2005. The occurrence or non-occurrence of contrail and cirrus formation within the sample area is related to several upper tropospheric variables through logistic regression techniques. Probabilistic models are developed to predict the occurrence of persistent linear contrails forming both with and without surrounding cirrus clouds. The forecast models provide insight into which atmospheric conditions are most susceptible to the formation of possible climate-altering contrails.

1 INTRODUCTION

Contrails and cirrus tend to form in similar (but not identical) atmospheric conditions, and thus it is difficult to determine how much persistent contrail coverage affects cirrus coverage. It is clear, however, that contrails that form imbedded in thick cirrus clouds will have little or no radiative impact on the atmosphere, while persistent contrails that form in otherwise clear skies will have a greater direct effect on climate. Although the atmospheric conditions necessary for cirrus and contrail formation are well known, the diagnosis or prediction of such clouds is still complicated by uncertainties in measuring the atmospheric state in the upper troposphere. Several high-resolution numerical weather analyses (NWA), including the Rapid Update Cycle (RUC; Benjamin et al., 2005a, 2005b) and the Advanced Regional Prediction System (ARPS; Xue et al., 2003), operate over the domain of the continental United States of America (USA). The main purpose of these models, however, is to predict the formation of storms and precipitation, and the meteorological accuracy necessary to predict persistent contrail formation directly from these models is not currently available. Duda et al. (2004) demonstrated that the RUC has a dry bias in the upper tropospheric humidity, and a strict diagnosis of persistent contrail formation from the Schmidt-Appleman criteria (Schumann, 1996) is problematic. In addition, numerical weather models are periodically modified and upgraded, leading to abrupt changes in the modelled relative humidity fields. Nevertheless, there appears to be a relationship between the vertical structure of the relative humidity fields represented in the numerical models and the lifetime, spreading rate, and optical depths of observed contrails. The results from Duda et al. (2004) show that the thickest, widest-spreading and longest-lasting contrails tend to occur in the model regions with the most upper tropospheric moisture. Hence, NWAs appear to have some useful meteorological information that could be used to forecast contrails and cirrus.

To deal with the limitations of the numerical weather analyses, probabilistic models that use statistics from the NWA to diagnose and forecast the occurrence of contrails and cirrus can be devel-

* *Corresponding author:* David Duda, National Institute of Aerospace, NASA Langley Research Center, MS 420, Hampton, VA 23681, USA. Email: dduda@nianet.org

oped for each version of a numerical weather model. Weather forecasters have used statistically post-processed numerical model output to make probabilistic forecasts for many years. One of the earliest models reported in the literature was developed by Lund (1955), and model output statistics (MOS; see Glahn and Lowry, 1972) were one of the first widely used probabilistic forecasts developed from numerical weather forecasts. Some probabilistic forecasts of contrail formation have also been published. Travis et al. (1997) used a combination of rawinsonde temperature and GOES (Geostationary Operational Environmental Satellite) 6.7 μm water vapour absorption data to develop a prognostic logistical model of the occurrence of widespread persistent contrail coverage. Jackson et al. (2001) created a statistical contrail prediction model using surface observations and rawinsonde measurements of temperature, humidity and winds over the New England states.

Because probabilistic forecasts use numerical model statistics to develop forecasts, they do not require the same level of meteorological accuracy necessary for classical cirrus and contrail formation theories, and new probabilistic forecast models can be developed as new versions of numerical models are implemented. Also, reliable probabilistic forecasts inherently have extra value to users compared to categorical (simple yes or no occurrence) forecasts because users can take advantage of cost/loss analyses better with probabilistic forecasts (Keith, 2003).

This paper presents a group of probabilistic models that predict the occurrence (or non-occurrence) of persistent linear contrails forming both with and without surrounding cirrus coverage, in an attempt to distinguish the atmospheric conditions that produce both contrails and cirrus from those that only produce contrails. The next section briefly describes the numerical weather models and the contrail observations used to develop the probabilistic models.

2 DATA

2.1 *Meteorological data*

Atmospheric profiles of temperature, humidity, horizontal wind speed and direction, and vertical velocity were derived from the 20-km resolution, hourly RUC analyses and 1-day, 2-day and 3-day forecasts from the ARPS in 25-hPa intervals from 400 hPa to 150 hPa. The ARPS data were obtained from the 27-km resolution, 1-hourly contiguous US domain analyses. Several other variables including the vertical shear of the horizontal wind and the temperature lapse rate were also calculated from the model data. These additional variables are expected to influence the spreading rate of persistent contrails (Jensen et al., 1998). Atmospheric humidity is expressed in the form of relative humidity with respect to ice (RHI). Due to computer storage limitations, the RUC and ARPS data were available at 1×1 degree resolution.

To match the meteorological data with observations of contrails, data from the RUC and ARPS analyses closest in time with the contrail observations are linearly interpolated to the location of each contrail observation. An observation was not used if the time difference between the contrail observation and the analyses was greater than 2 hours (nearly all pairs matched to within 1 hour).

2.2 *Surface data*

Observations of contrail and cirrus occurrence and coverage across the contiguous USA were collected from primary and secondary schools across the country by the Global Learning and Observations to Benefit the Environment (GLOBE) program (see www.globe.gov for more information about the GLOBE program.). In May 2003, GLOBE initiated the contrail observation protocol to gather and classify contrail observations. A primary goal of the GLOBE program is to use detailed written protocols to enable students to provide scientifically valuable measurements of environmental parameters (Brooks and Mims, 2001). Over 14,600 observations were reported over the region between May 2004 and June 2005. They include contrail coverage, contrail number, cloud coverage, cloud type and a classification of contrails into three categories; short-lived, non-spreading persistent contrails, and spreading persistent contrails. A subset of 10 stations (see Figure 1) with at least 50 contrail observations under mostly clear skies (cloud coverage less than 25 percent) was chosen for building some of the probabilistic models.

2.3 *Satellite data*

To supplement the meteorological data from the NWAs, radiance data from the 6.7-μm water vapour absorption channel on *GOES-12* were also used as atmospheric predictors of contrail formation. The 6.7-μm channel is sensitive to the top three millimetres of water vapour profile in the atmospheric column, and most of the detected emission is from the layer between 500 to 200 hPa (Travis et al., 1997; COMET, 2002), with peak sensitivity near 400 hPa. Both the raw water vapour image counts and the calibrated 6.7-μm brightness temperature were collected.

In addition to the GOES data, multi-spectral measurements taken by the NOAA-16 Advanced Very High Resolution Radiometer (AVHRR) provided observations of contrail occurrence. Five hundred twenty-five afternoon overpasses were collected for a 4 by 6 degree area centred over the states of Ohio, western Pennsylvania and West Virginia (from 38°N to 42°N, and 84°W to 78°W). For each 1 by 1 degree grid box within the sample area, persistent contrails and cirrus were detected from the satellite radiances. The contrails were detected using the automated procedure of Mannstein et al. (1999), while the cirrus were identified from a visual inspection of the 10.8 μm brightness temperature data, and the 10.8 μm minus 12.0 μm brightness temperature difference measurements. To reduce the number of contrail false detections due to cloud street formations, the satellite viewing angle for each overpass was required to be less than 50 degrees. Although each 1 by 1 degree grid box provides one observation of contrails and cirrus, due to gaps in the availability of the datasets and the viewing angle restrictions, only about 6000 observations were possible from the satellite overpasses.

3 MODEL DEVELOPMENT

3.1 *Data pre-processing*

Nearly 15 months (April 2004 – 27 June 2005) of meteorological data from the RUC and ARPS were collected each day to a local computer. (After 12 UTC on 28 June 2005, the 13-km resolution version of the RUC model began operation, with significant differences in upper tropospheric humidity.) The data are subject to interruptions including computer and power failures, full disks, operator errors and other problems. Thus, approximately 77% of the hourly ARPS data was collected and 99.7% of the RUC data was collected during the time period. Two large gaps (between 20 August – 28 September 2004, and between 21 January – 21 February 2005) accounted for nearly 85% of the ARPS data loss.

The collected data were separated into a dependent (from which the statistical model was created) and an independent (on which the model was tested) dataset. Two-thirds of the observations were randomly selected to build the dependent dataset, while the independent dataset comprises the remaining one-third of the observations.

Before deriving the statistical forecast equations, the NWA data are checked for missing data. None of the missing data were replaced by surrogate values (such as persistence, interpolation or nearest-neighbour techniques) because this study focuses on the general meteorological conditions necessary for persistent contrail formation across the United States, rather than forecasting contrail formation for any particular time or location.

3.2 *Statistical technique*

Logistic regression (Hosmer and Lemeshow, 1989) was used to create a probabilistic estimate of persistent contrail formation. Logistic regression techniques are commonly used where the predictand, such as in this case, is a dichotomous (yes/no) variable. Two advantages of logistic regression compared with multiple linear regression are that the forecast values cannot fall outside of the 0 – 1 probability range, and that each predictor can be fit in a nonlinearly way to the predictand. The logistic model assumes the following fit in Equation 1:

$$P \approx \frac{1}{1+\exp[-(\beta_0+\beta_1 x_1+\cdots+\beta_p x_p)]}. \quad (1)$$

P is the predictand (probability of persistent contrail formation) and β_i (for $i = 1,\ldots, p$) are the set of coefficients used to fit the predictors (x_i) to the model.

The predictors x_1, x_2, x_3,…,x_n are atmospheric variables derived from NWA and satellite measurements. A set of up to 80 possible predictors were tested. All predictors used in this study were based on meteorological quantities in the upper troposphere that are suspected to be related to the formation of spreading, persistent contrails including humidity, temperature, vertical velocity, wind shear, wind direction and atmospheric stability. GOES water vapour channel data were also used as predictors for some regressions.

The maximum likelihood method was used to estimate the unknown coefficients β_i and fit the logistic regression model to the data. The chi-square statistic (χ^2) was used to assess the goodness of fit of each logistic model to the NWA data. A total from 55 to 80 potential predictors from the RUC and ARPS models respectively were used to develop the statistical contrail model. To reduce the number of predictors to an optimal number, a forward stepwise regression technique was used. In each step of the technique, a new predictor is added to the logistic model and the chi-square statistic is compared with the previous model. The new predictor that produces the largest improvement in model fit (that is, the largest increase in χ^2) is added to the model. To avoid over-fitting of the dependent dataset, the stepwise regression technique is allowed to add predictors to the model until the test for statistical significance reaches a significance level (i.e. p-value) of 0.05. The stepwise technique usually resulted in 6 to 11 predictors for each model. Separate regressions were computed for 4 dependent variable scenarios. The scenarios include:

- Both contrails and cirrus form
- Only cirrus clouds form
- Only linear contrails form
- No cirrus or contrails form

As mentioned above, several meteorological variables were considered as predictors in the development of the statistical forecast model. In addition, several combinations of meteorological variables (such as temperature × humidity) were also considered to account for interactions between variables.

3.3 *Skill scores*

As a simple method to assess the skill of the contrail/cirrus forecasts, the probabilistic forecasts were converted into categorical (i.e. yes/no, occurrence/non-occurrence) forecasts by simply forecasting the occurrence of the dependent variable when the probability was greater than or equal to 0.5, and forecasting non-occurrence when the probability was less than 0.5. A variety of statistical measures have been developed to evaluate the accuracy of categorical forecasts. Several of these have been used to measure the success of previous contrail formation forecasts (Jackson et al., 2001; Walters et al., 2000). The contrail formation forecasts are separated into four categories based on the forecast and its outcome: a is the number of cases where persistent contrail formation is forecasted and persistent contrails are observed (hits); b is the number of cases where contrails are predicted, but no contrails are observed (false alarms); c is the number of cases where contrails are not forecasted, but contrail are observed (misses); and d is the number of cases where contrails are not forecasted and no contrails are observed (correct rejections). Two of the measures are:

- Hit rate. The hit rate is calculated as $(a + d)/(a + b + c + d)$ and represents the percentage of forecasts in which the method correctly predicted the observed event.
- Heidke Skill Score (HSS). The HSS is calculated as $HSS = 2(ad – bc) / [(a + c)(c + d) - (a + b)(b + d)]$ (Wilks, 1995). This measure of forecasting skill compares the hit rate of the forecast method with the hit rate achieved with a random forecast. Perfect forecasts have an HSS of one, forecasts equal in skill to the random forecast have an HSS of zero, while a negative HSS indicates that the forecasts are less skillful than random forecasts.

4 RESULTS AND CONCLUSIONS

The most important predictors chosen in the logistic models (both those developed from the surface observations (not shown) and those developed from the satellite observations) tended to be related to temperature and humidity. Other variables including vertical velocity, wind direction and speed,

wind shear, and the altitude of maximum RHI were also common predictors. Table 1 shows the hit rates and Heidke skill scores from the models developed using the NOAA-16 cirrus and contrail observations. In all four scenarios for both the RUC and ARPS the hit rates are about 0.75 or greater. The best skill scores occur when both cirrus and contrails appear together, or no high cloudiness is observed.

The lack of skill indicated for the contrail-only models is mainly the result of having relatively few examples of grid boxes with only contrails visible (less than 15 percent of the total), and the nature of the atmospheric conditions in regions where contrails form in the absence of cirrus. The contrail-only grid boxes tend to occur at the edges of areas of high humidity and cooler tropospheric temperatures, and the exact locations of these regions are not always represented well in the numerical models. Also, the contrail detection results have not been checked for the possibility of false positive results due to cloud streets and other linear cloud features unrelated to contrails. Increasing the number of contrail-only cases and refining the contrail and cirrus detection results would allow for more accurate models and improved skill scores for the contrail-only scenario.

Table 1. Hit rates and skill scores from satellite observations over Ohio, Pennsylvania and West Virginia.

Scenario	Hit Rate	Skill Score
RUC (both CT/Ci)	0.74	0.32
ARPS (both CT/Ci)	0.76	0.37
RUC (cirrus only)	0.83	0.20
ARPS (cirrus only)	0.82	0.15
RUC (contrails only)	0.86	0.00
ARPS (contrails only)	0.86	0.02
RUC (no CT/Ci)	0.75	0.46
ARPS (no CT/Ci)	0.76	0.50

The most common predictors in the scenarios with the best overall skill scores (both CT/Ci and no CT/Ci) are variables related to temperature and humidity. For the "both CT/Ci" scenario, the most common predictors are temperature, RHI, temperature × RHI, and vertical velocity, while for the "no CT/Ci" scenario the most common predictors are temperature^2, RHI^2, temperature × RHI, the altitude of maximum RHI, and wind direction. The differences in common predictors chosen for each scenario suggest that some meteorological quantities are especially useful in determining regions of upper tropospheric cloudiness. Cirrus and contrails are likely to form in regions of positive vertical velocities, while the absence of high clouds is often indicated by the overall synoptic conditions that control wind direction and humidity within the upper troposphere. These results show that current numerical weather analyses describe the atmospheric state in the upper troposphere with sufficient accuracy to locate potential regions of contrail and cirrus formation within a region as small as 1 degree by 1 degree.

An example of multi-variable logistic regression was presented to address some of the limitations of using operational numerical weather prediction models in the diagnosis and prediction of contrail and cirrus cloud formation. More work is necessary to refine the accuracy of the contrail and cirrus observations. More specifically, more quality control work is needed with the contrail detection algorithm to eliminate false positives, and the use of the objective GOES-based gridded cloud products can improve estimates of cirrus occurrence. Techniques like logistic regression may be helpful in discovering robust relationships between the atmospheric variables represented in numerical models and the formation of cirrus and contrails in the atmosphere.

ACKNOWLEDGEMENTS

This material is based upon work supported by the NASA Earth Science Enterprise Radiation Sciences Division, NASA contracts NAG1-02044, NCCI-02043, and NIA-2579, and by the National Science Foundation under Grant No. 0222623.

REFERENCES

Benjamin, S. G., G. A. Grell, J. M. Brown, T. G. Smirnova, and R. Bleck, 2004a: Mesoscale weather prediction with the RUC hybrid isentropic-terrain-following coordinate model. *Mon. Wea. Rev.*, *132,* 473–494.

Benjamin, S. G., D. Dévényi, S. S. Weygandt, K. J. Brundage, J. M. Brown, G. A. Grell, D. Kim, B. E. Schwartz, T. G. Smirnova, T. L. Smith, and G. S. Manikin, 2004b: An hourly assimilation-forecast cycle: The RUC. *Mon. Wea. Rev.*, *132,* 495–518.

Brooks, D. R., and F. M. Mims III, 2001: Development of an inexpensive handheld LED-based Sun photometer for the GLOBE program. *J. Geophys. Res., 106(D5),* 4733–4740.

COMET, 2002: Satellite meteorology: GOES channel selection. http://meted.ucar.edu/satmet/goeschan/print/print.htm

Duda, D. P., P. Minnis, L. Nguyen, R. Palikonda, 2004: A case study of the development of contrail clusters over the Great Lakes. *J. Atmos. Sci.*, *61,* 1132–1146.

Glahn, H. R., D. A. Lowry, 1972: The use of model output statistics (MOS) in objective weather forecasting. *J. Appl. Meteorol., 11,* 1203–1211.

Hosmer, D. W., and S. Lemeshow, 1989: *Applied Logistic Regression.* John Wiley & Sons, New York, 307 pp.

Jackson, A., B. Newton, D. Hahn, A. Bussey, 2001: Statistical contrail forecasting. *J. Appl. Meteorol., 40,* 269–279.

Jensen, E. J., A. S. Ackerman, D. E. Stevens, O. B. Toon, and P. Minnis, 1998: Spreading and growth of contrails in a sheared environment. *J. Geophys. Res., 103,* 31,557–31,567.

Keith, R., 2003: Optimization of value of aerodrome forecasts. *Weather and Forecasting, 18,* 808–824.

Lund, I. A., 1955: Estimating the probability of a future event form dichotomously classified predictors. *Bull. Amer. Meteorol. Soc., 36,* 325–328.

Mannstein, H., R. Meyer, P. Wendling, 1999: Operational detection of contrails from NOAA-AVHRR data. *Int. J. Remote Sensing, 20,* 1641–1660.

Schumann, U., 1996: On conditions for contrail formation from aircraft exhausts. *Meteorologische Zeitschrift, 5,* 4–23.

Travis, D. J., A. M. Carleton, S. A. Changnon, 1997: An empirical model to predict widespread occurrences of contrails. *J. Appl. Meteor., 36,* 1211–1220.

Walters, M. K., J. D. Shull, J. P. Asbury III, 2000: A comparison of exhaust condensation trail forecast algorithms at low relative humidity. *J. Appl. Meteor., 39,* 80–91.

Wilks, D. S., 1995: *Statistical Methods in the Atmospheric Sciences.* Academic Press, 467 pp.

Xue, M., D. –H. Wang, J. –D. Gao, K. Brewster, and K. K. Droegemeier, 2003: The Advanced Regional Prediction System (ARPS), storm-scale numerical weather prediction and data assimilation. *Meteor. Atmos. Physics, 82,* 139–170.

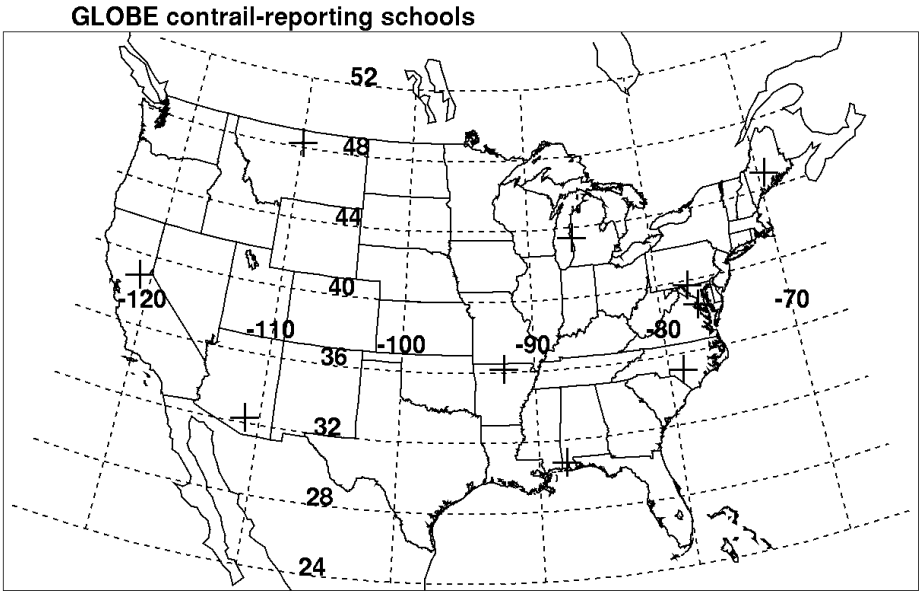

Figure 1: Location of contrail-reporting schools in the United States of America used in the development of logistic regression models.